An Electron Microscopy Investigation of the Transient Stage Oxidation Products in an Fe-22Cr Alloy with Ce and La Additions Exposed to Dry Air at 1073 K (800 °C)

JINGXI ZHU, LAURA M. FERNÁNDEZ DÍAZ, GORDON R. HOLCOMB, PAUL D. JABLONSKI, CHRISTOPHER J. COWEN, DAVID E. ALMAN, DAVID E. LAUGHLIN, and SEETHARAMAN SRIDHAR

In this study, the effects of Ce (270 ppm) and La (120 ppm) mischmetal additions on the transient oxidation of an Fe-22Cr alloy were investigated. The oxidation process was imaged *in situ* using a confocal scanning laser microscope. The oxidation microstructures were studied by scanning electron microscopy, energy dispersive X-ray analysis, and transmission electron microscopy with the help of focused ion beam *in situ* lift-out specimen preparation. The Ce and La, referred to as reactive elements, were found in nonmetallic inclusion particles in the forms of oxides, sulfides, and phosphates. An affected zone formed around rare earth (RE)-containing inclusion particles at the alloy free surface during the transient oxidation. This zone consisted of an internal Cr-oxide formed beneath the particle as well as a thinner external oxide scale on the surface compared with the surroundings. The relation of this microstructure to oxidation kinetics is discussed. With time, the RE elements diffused into the scale from the RE particles on the alloy surface during the high-temperature exposure. A diffusion mechanism is presented to describe these observations.

DOI: 10.1007/s11661-010-0493-y

I. INTRODUCTION

To commercialize solid oxide fuel cell (SOFC) technologies, Fe-Cr based alloys (less than 24 wt pct Cr) are favored candidates for the metallic interconnector in planar design cells.[1] The flat plate (planar) design into which these materials are to be incorporated is favored because of the ease of processing and manufacturing of the cell components.[2] Metallic interconnectors in the SOFC stack provide mechanical support to the cell components, sealing between the fuel and oxygen/air sides and the electrical contact between single cells. Ceramic oxides based on doped lanthanum chromite and relatively expensive high-Cr superalloys have been used previously as interconnector materials.[1] However, lowering of the operational temperature of SOFCs from approximately 1273 K to 1073 K (1000 °C to 800 °C), offers the possibility of using less expensive alloys, such as Fe-Cr alloys. Fe-Cr alloys with Cr contents less than 24 wt pct offer a cost-effective alternative with excellent electrical conductivity through the Cr_2O_3 scale that is relatively protective. Also, the thermal expansion coefficient of this alloy class more closely matches that of the other components within the cell; these properties make Fe-Cr alloys favorable candidates for interconnector materials.[1,3] Research has been carried out on potential Fe-Cr alloys including Crofer 22[4,5] developed by Hojda *et al.*[6] by adding Mn, Ti, and La to an Fe-20~24Cr base alloy and the commercially available 444[7,8] stainless steel. Because of its higher Cr content, Crofer 22 has a better oxidation resistance than the 444 stainless steel.

A major problem with metallic interconnectors based on Fe-Cr alloys, is their reactivity with the electrode service environments at operating temperatures. The resulting high-temperature corrosion or oxidation can lead to the failure of the cell. Also, volatile chromium oxides (*e.g.*, CrO_3 and $CrO_2(OH)_2$) can form at the oxide scale/oxidant interface, migrate to the cathode/electrolyte interface, and form Cr_2O_3 deposits, which can poison the cathode reaction and reduce SOFC efficiencies.

The oxidation of metals and alloys takes place by either outward diffusion of cations or the inward diffusion of oxygen anions through the oxide scale.[9,10]

JINGXI ZHU, PhD Student, is with the Department of Materials Sciences and Engineering, Carnegie Mellon University, Pittsburgh, PA 15213 and the National Energy Technology Laboratory, Pittsburgh, PA 15236. Contact e-mail: jingxiz@andrew.cmu.edu LAURA M. FERNÁNDEZ DÍAZ, formerly with the Department of Materials Science and Engineering, Carnegie Mellon University and the National Energy Technology Laboratory, is now Postdoctoral Researcher with Physics Institute, National University of Mexico, México City 04510, Mexico. GORDON R. HOLCOMB, Materials Research Engineer, PAUL D. JABLONSKI, Metallurgist, CHRISTOPHER J. COWEN, Materials Research Engineer, and DAVID E. ALMAN, Division Director, Materials Performance Division, Office of Research and Development, are with the National Energy Technology Laboratory, Albany, OR 97321. DAVID E. LAUGHLIN, ALCOA Professor of Physical Metallurgy, is with the Department of Materials Sciences and Engineering, Carnegie Mellon University. SEETHARAMAN SRIDHAR, POSCO Professor of Materials Science and Engineering, the Department of Materials Sciences and Engineering, Carnegie Mellon University, Pittsburgh, PA 15213 and NETL Resident Faculty Fellow with the National Energy Technology Laboratory, Pittsburgh, PA 15236.

Manuscript submitted May 25, 2010.
Article published online October 19, 2010

The outward diffusion of metal normally results in the formation of an external scale that grows at the scale/gas interface as well as in the formation of voids and cavities at the scale/alloy interface that can lead to the scale spallation. In many cases, it is the properties of this external scale that determine the oxidation resistance of the alloy. Many studies have been carried out to understand the high-temperature oxidation mechanism and to improve the oxidation resistance of Fe-Cr alloys. It has been reported that when reactive elements—the most commonly used are rare earth (RE) elements such as La and Ce—were added to Fe-Cr alloys, the scale no longer grew by outward diffusion of Cr but by inward diffusion of oxygen, which significantly reduced the scale growth rate and improved the scale adhesion,[11] and this phenomenon was dubbed the "reactive element effect" (REE).

The so-called REE was first patented in 1937 by Pfeil.[12] The original work concerned cerium additions to a Ni-Cr alloy, but since then the same effect has been found for a wide variety of elements with a high affinity for oxygen and sulfur (reactive elements), and benefits are reported for most chromia- and alumina-forming alloys, including Fe-Cr ferritic stainless steels. Several REEs for chromia scales have been claimed and were reviewed by D.P. Whittle and J. Stringer.[11] The REE is made up of many different factors, some of which are clearly interrelated and include the following: increased selective Cr oxidation, reduced growth rate of the scale, promotion of oxygen anion transport, suppression of void formation at the interface, and increased adhesion of the scale and reduction of the scale grain size.

Although many mechanisms have been proposed to explain the REE, explanations by different authors are not in complete agreement with one another, such as segregation models *vs* doping models. One of the difficulties encountered in attempting to verify the various hypotheses that have been made concerning the mechanisms whereby RE elements affect the growth and adhesion of chromium oxide scales is that the location and form of RE elements in chromium oxide scales have not been established completely. Several investigations have suggested that the role of the RE is to block fast-path transport paths through grain boundaries of the cations (*e.g.*, Reference 13), and the presence of RE at grain boundaries of alumina scale recently was measured experimentally by B. Tang *et al.*[14]

It is also uncertain with regard to whether the mechanisms of the REE are the same for RE elements in the metallic addition to the bulk as compared with the surface enrichment of a stable RE compound.[11]

The current study focused on the REE in alloys with metallic RE additions and their behavior during the transient oxidation of such alloys. As the result of the metallic additions during the melt processing, the RE elements existed in the alloy either as RE inclusions after gettering various impurities in the melt or as dissolved RE elements in the metal matrix. The current investigation aims to document the evolution of nonmetallic RE inclusion particles and the nearby scale/alloy microstructure as a function of oxidation time to establish the following: (1) whether the particles serve as sources of RE that migrate into the Cr-oxide scale, (2) whether such a source is long-lived enough to influence oxidation beyond the transient stage, and (3) where the RE elements from these sources are concentrated.

The alloy studied in the present investigation is similar to a Crofer 22 alloy with 22 wt pct Cr, in which Ce and La were added before the melt was cast. The specific mass change of this alloy in a 2000-hour exposure in moist air at 1073 K (800 °C) was compared with the alloy of the same chemistry but without a RE addition in which a significant reduction of oxidation rate was found with the addition of La and Ce.[15]

II. EXPERIMENTAL

A. *Sample Preparation*

All test samples were manufactured at the National Energy Technology Laboratory (NETL) of the U.S. Department of Energy. An Fe-22 wt pct Cr ferritic stainless steel was selected as the base material and was produced in-house at the NETL's Albany, OR site. Vacuum induction melting was used to produce 7-kg ingots from high-purity starting elemental materials. After casting, the alloys were reduced to a sheet by hot working and cold rolling.

A misch-metal addition of RE elements was added to the melt before the casting of the ingots. Glow-discharge mass spectroscopy was used to analyze the RE elemental content of the alloy, as summarized in Table I. Most RE added was Ce and La. The RE-containing inclusion particles in the alloy contained one or several of the following phases: RE oxides, sulfides, oxysulfides, phosphides, and oxyphosphides. A more quantitative description of the RE-containing inclusion particles will be given in Section III–D–1 in terms of their size and chemistry.

The samples to be oxidized were cut into 5 mm × 5 mm × 1 mm pieces, ground through a 1200-grit finish, and fine polished with 6-, 3-, and 1-μm diamond suspensions. The polished samples subsequently were cleaned with soapy water and cleaned ultrasonically in acetone and ethanol.

B. *High-Temperature Experiments*

Because rapid heating and cooling rates are essential to study transient oxidation, samples were oxidized in a hot stage attached to a confocal scanning laser microscope (CSLM). The hot stage comprises a halogen lamp and an ellipsoid-shaped gold-image furnace that can reflect the radiation from the halogen lamp (located at the lower focus of the ellipsoid) as well as concentrate the radiation on the sample placed in the crucible (upper focus of the ellipsoid). With this design, the furnace can achieve a high heating rate; for example, heating from room

Table I. Composition of the Study Alloys (Weight Percent)

	Cr	C	Mn	Ti	La	Ce
F2	22.12	0.005	0.55	0.072	0.012	0.027
F3	22.19	0.019	0.56	0.77	0.029	0.061

temperature to 1073 K (800 °C) takes approximately 45 seconds. A schematic drawing of the gold-imaging furnace and a description of the contrast formation with confocal optics can be found in Reference 16.

The temperature of the sample during the high-temperature exposure is measured by a thermocouple placed near the sample surface. The measured temperature is used to control the heating intensity and is always calibrated with a pure metal of known melting temperature before the actual exposure. The temperature profile of the oxidation experiment is programmed prior to oxidation.

To remove the possible build-up of moisture in the furnace chamber, the chamber was evacuated before every oxidation experiment and refilled with dry air, which subsequently was allowed to flow for 5 minutes. This evacuation-and-refilling step was repeated three times. The flow rate of dry air was controlled at 500 ml/min during the high-temperature exposure. The samples were heated from room temperature to 1073 K (800 °C) in 45 seconds, and then the samples were maintained at 1073 K (800 °C) isothermally for a designated time interval followed by cooling to room temperature within 45 seconds. The surface of the sample was imaged continuously at a rate of 30 frames/s to document topographical changes that occurred during oxidation. All samples examined in this study were oxidized under the aforementioned conditions. The oxidized samples then were used for characterization.

C. *Characterization*

The evolution of microstructures of RE-containing features has been investigated via characterizing the samples both before and after the high-temperature oxidation in addition to *in situ* observations in the confocal microscope mentioned in Section II–B. In the current study, various characterization methods that have been applied are described in Sections II–C–1 through II–C–3.

1. *Scanning electron microscopy (SEM) and focused ion beam (FIB)*

The oxidized as well as the nonoxidized surfaces of the samples were examined in a Philips XL 30 (Royal Philips Electronics, Netherlands), field emission scanning electron microscope (SEM) equipped with an Oxford INCA (Oxford Instruments, Tubney Woods, UK) energy dispersive X-ray analysis (EDX) detector. After the plane view characterizations of the samples, cross-sectional characterizations were performed. Cross sections were obtained by milling a rectangular hole (ca. 10×5 μm) into the surface with a Nova 600 DualBeam system (FEI Company, Eindhoven, Netherlands) (electron beam/focused ion beam [FIB]). An initial Pt layer 10-nm thick was made with plasma deposition to avoid damage from imaging with the ion beam. Subsequently, a 1 to 2-μm thick Pt strip was deposited onto the region of interest to be cross sectioned (approximately 20 μm in width) before milling. The surface then was cross sectioned to the desired depth using a 30-kV Ga^+ ion beam with a current of ca. 0.5 nA.

2. *FIB in situ lift-out transmission electron microscopy (TEM) specimen preparation*

To study the evolution of the microstructure of the scales formed after high-temperature exposure and more importantly to study the evolution of the location of particles containing the RE with respect to their changing surroundings during oxidation, regions containing RE particles were made into TEM specimens by the FIB *in situ* lift-out technique.

The FIB *in situ* lift-out TEM specimens were prepared as follows: First, two deep trenches ($25 \times 10 \times 15$ μm) were milled on both sides of the site of interest. The lamella between the two trenches then was detached from the bulk material so that only two thin bridges connected to the top of the lamella remained to support it. Next, the Omniprobe was inserted into the chamber, and the lamella was attached to the probe needle with Pt deposition. After the lamella was welded to the needle, the two bridges that were supporting the lamella were cut to free the lamella entirely. The freed lamella ($15 \times 10 \times 2$ μm) therefore could be lifted from the substrate and welded to a Cu grid by Pt deposition. Finally, the probe needle was detached from the welded lamella and retracted, and the lamella was thinned to less than 100 nm after normal FIB TEM sample preparation procedures.

3. *TEM*

A Philips Tecnai F20 FEG TEM (Royal Philips Electronics, Netherlands) was used for microscale investigation in this study. The Tecnai has a field-emission electron source and was operated at an accelerating voltage of 200 kV. An EDAX (Ametek Inc, Paoli, PA) energy dispersive X-ray analysis system is installed in the Tecnai. The software can be used to collect scanning transmission electron microscopy (STEM) high-angle annular dark-field (HAADF) images, EDX maps, EDX line profiles, and EDX spot analyses. The electron-transparent windows that were prepared using the DualBeam system were analyzed via a combination of these techniques. (The two-layered Pt deposition previously mentioned appeared as two distinct bright layers in STEM-HAADF images and as two dark layers in conventional transmission electron microscope [CTEM] bright-field images.) Spot sizes of 1 nm were used for line scans and spot analyses. The quantitative results are presented in integrated intensities.

III. RESULTS

The scale growth was visualized in the CLSM, and the scale was characterized with SEM-EDX, SEM-FIB, and TEM after oxidation. The results in this section were obtained from F2 (Fe-22Cr-0.04RE) and F3 (Fe-22Cr-0.08RE) alloys that underwent transient isothermal oxidation at 1073 K (800 °C).

A. *General Scale Morphology After Transient Oxidation*

The morphologies of the scales grown on the F2 alloy after 15 minutes of exposure are shown in Figure 1.

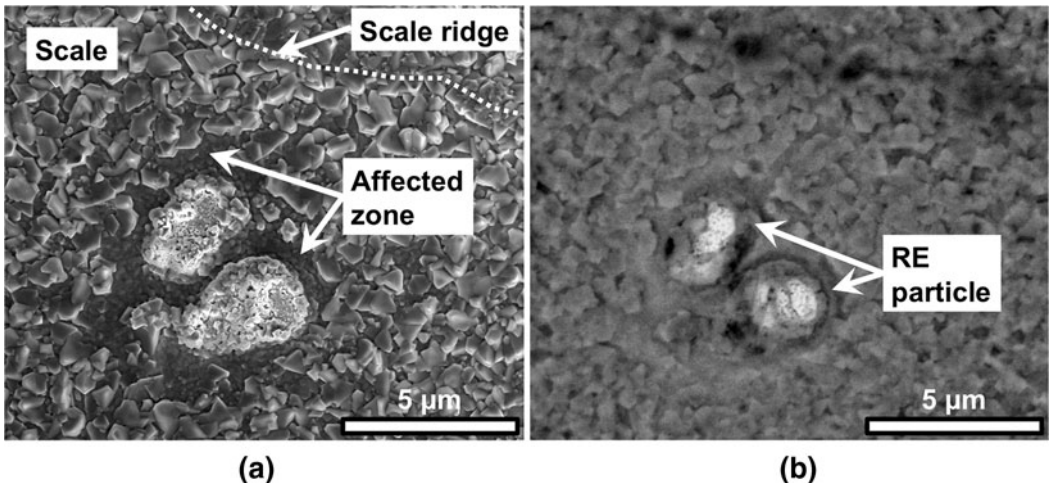

Fig. 1—Plane view (*a*) secondary electron image and (*b*) backscattered electron image of scale layer grown on sample F2 oxidized for 15 min at 1073 K (800 °C) in dry air.

Instead of a uniform scale layer, heterogeneities were found on the scale in the forms of scale ridges (dotted line), RE inclusion particles, and the scale around the RE particles.

The fast grain-boundary diffusion of the scale-forming elements resulted in the formation of scale ridges,[17] and the relation between scale ridges and alloy grain-boundary characteristics has been analyzed in Reference 16.

RE inclusion particles can be found on the sample surface after oxidation with a distinct scale feature around them. The scale oxide grain size around the RE particles was much smaller than that of the scale away from the RE particles. This area with smaller oxide grains was named the "affected zone" (Figure 1). A cross-sectional analysis also showed that the scale in the affected zone was thinner than the scale outside the zone. Investigation into the RE particles and the affected zone revealed their possible relation to the REE, which will be discussed in Section IV–A.

B. *Transient Stage Scale and RE Particles*

As mentioned before, as the result of the metallic additions during the melting stage, the RE elements existed in the alloy either as RE inclusions after gettering various impurities, such as O, P, and S in the melt, or as dissolved RE elements in the metal matrix. However, because of the relatively small solubility of RE elements in the metal matrix and their reactivity, much of the RE added into the alloy was contained in the RE inclusions.[18] Therefore, regardless of whether the dissolved RE plays a role in the REE, a detailed study on the behavior and the evolving dynamics of these elements in the inclusions after oxidation should give an indication of whether the RE elements in the inclusions particles are related to the observed REE. To examine whether an interaction took place between the RE inclusion particles and the oxide scale in contact with such particles, the scale evolution was studied first.

C. *Scale Evolution as a Function of Time*

The scale morphology after 15, 30, and 60 minutes of exposure to dry air at 1073 K (800 °C) of the F2 alloy is shown in Figure 2. A fair number of oxide grains (up to 60 minutes of oxidation, Figure 2) seem to be faceted platelet crystals. The latter would provide a large amount of surface area for a gas/metal reaction. With higher magnification, it was revealed that many oxide crystals typically grew by ledges (*e.g.*, Figure 3) on the surfaces of the planar facets of the individual grains. By such ledge growth, new oxide can grow with a much lower resulting increase in the interfacial energy than through nucleation on a flat surface.[19] Transport of metal cations is fast during the transient stage when the external scale is thin,[10] and therefore, gas phase transport of oxygen molecules, adsorption, and/or dissociation would be expected to be rate controlling and to result in a linear rate. Metal cations may react at ledge sites where oxygen might be readily adsorbed and dissociate. Therefore, the ledge growth observed on the scale suggests that the gas/metal reaction takes place at the surface of the oxide grains, and therefore, the scale grows outward. As oxidation and grain growth proceeded, the oxide grains impinged and closed the gaps between oxide grains, which is shown when comparing Figure 2(a) with Figures 2(b) and (c). This finding can be interpreted as a transition in scale growth from gas phase mass transfer to grain boundary diffusion of metal ions, which also can be considered a transition from transient state to steady-state oxidation. Grain-boundary diffusion of chromium ions was considered in a previous study to be the main mechanism of steady scale growth on a chromia-forming alloy.[20]

Based on the cross-sectional micrographs in Figure 4, it is shown that, while continuing to grow larger, the oxide grains after 60 minutes of oxidation clearly show the tendency of growing into columnar grains (each grain is single crystal in nature) because many oxide grain boundaries are close to being perpendicular to the scale/alloy interface and the scale surface, as well as connecting the two interfaces, as indicated by the arrows

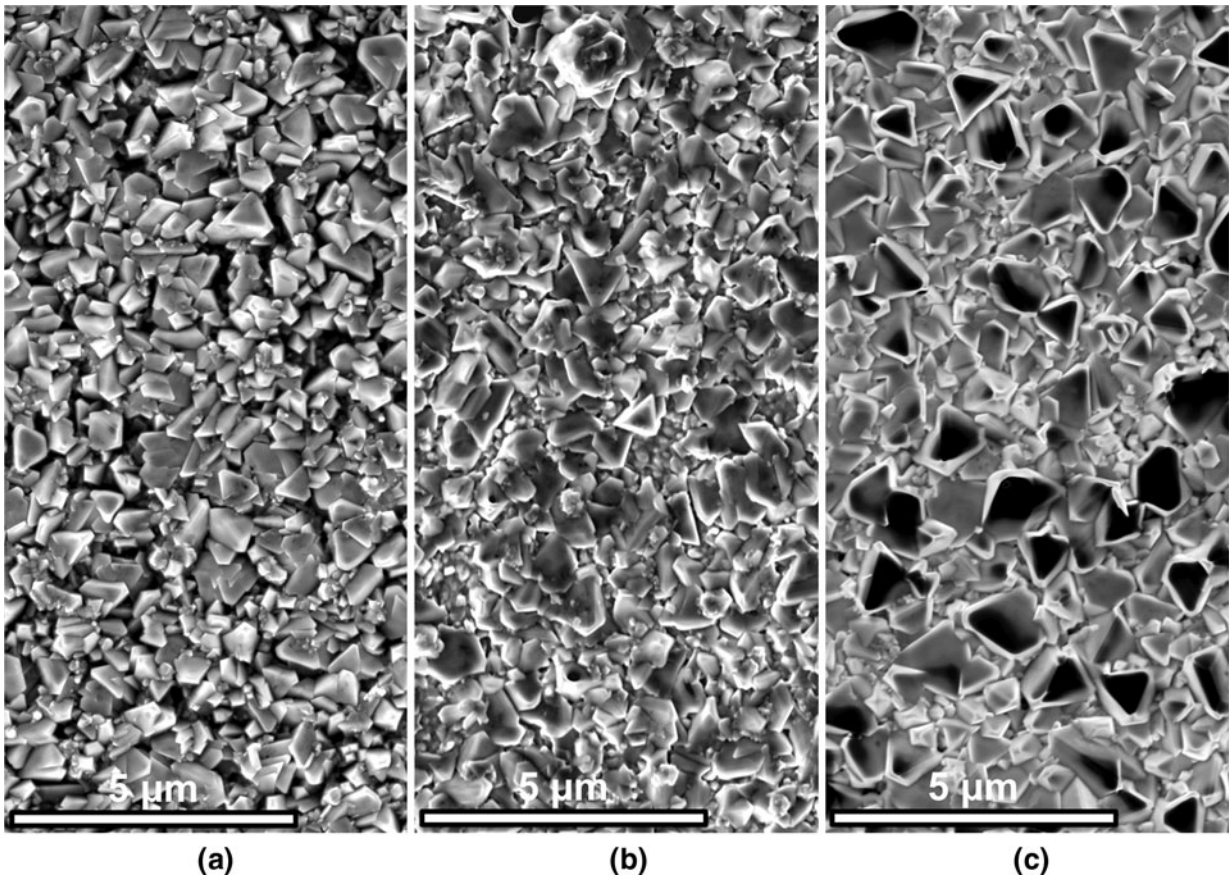

Fig. 2—Plane view secondary electron images of scales grown on sample F2 oxidized for 15 min (*a*), 30 min (*b*), and 60 min (*c*) at 1073 K (800 °C) in dry air.

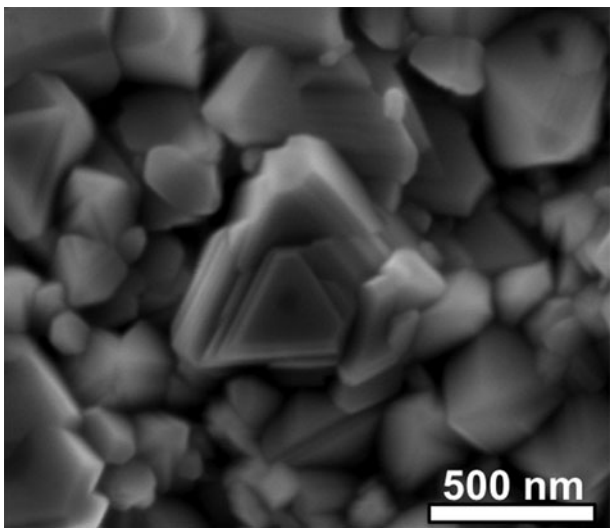

Fig. 3—Planeview secondary electron image of oxide grains after 15-min exposure. Notice the steps on the platelet grain in the center of the micrograph.

in Figure 4. Columnar oxide grains commonly have been observed on alloys oxidized for a relatively long time.[21] It will be shown in Section IV–B–1 that oxide grain morphology in the scale is important for the behavior of RE in the scale.

D. *RE-Containing Inclusion Particles*

1. *RE inclusion particles on the sample surface of alloy F2 before oxidation*

First, the RE inclusion particles on the sample surface before high-temperature exposure were analyzed statistically using SEM-EDX. Summarizing the statistical results showed the following:

(a) The particle sizes ranged from 0.5 μm to 2.5 μm, and no clear trend between the chemistry and the size (and aspect ratio) of the particles was found. The median particle size was around 1 μm in diameter.
(b) The density of RE inclusions was approximately one inclusion per 1000 μm^2 on the surface of an F2 alloy.
(c) RE oxides, sulfides, oxysulfides, phosphides, and oxyphosphides were found, and about half of the particles also contained a certain amount of Ti (0.8–3.6 wt pct).
(d) The inclusions were mostly spheroids or ellipsoid-shaped particles comprising one or several of the aforementioned compounds, enriching in different parts within the particle. One example of such RE particles is shown in Figure 5(a), which can be divided into four regions according to the constituent compounds as detailed in Figure 5(b).

Assuming the particles to be pure CeO_2, a simple estimate of the Ce content of the alloy can be made

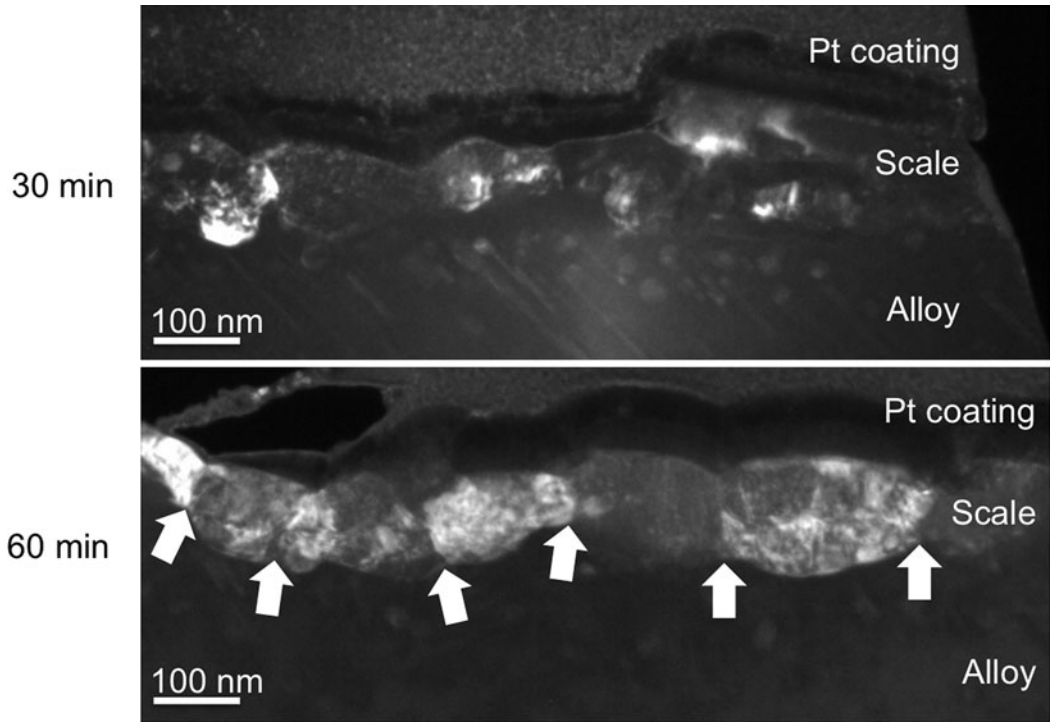

Fig. 4—Conical dark-field cross-sectional image of the external scale formed on F2 (Fe-22Cr-0.04RE) after 30 min and 60 min of high-temperature exposure.

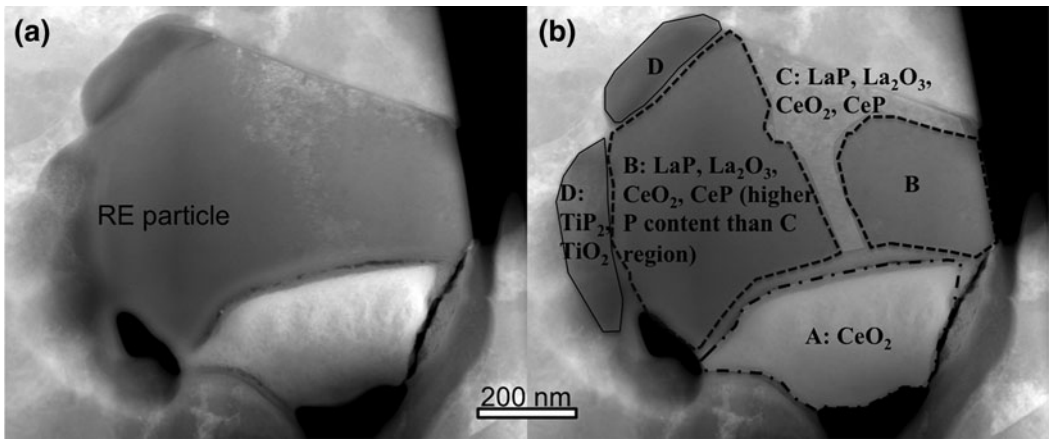

Fig. 5—(*a*) Cross-sectional STEM-HAADF image of a RE particle before oxidation. (*b*) The RE particle divided into four regions according to the chemical composition and the compounds present.

based on the alloy and oxide densities as well as on the apparent particle size and area fraction. Such an estimate was made resulting in approximately 80 ppm Ce, much below that of the alloy (270 ppm). Thus, it is probable that not all Ce was tied up in these particles prior to oxidation.

Although the RE inclusion particles appeared as micronsized particles, the TEM image together with electron diffraction indicated that these large RE particles were made up of a large amount of nanosized grains, such as the particle shown in Figure 6.

It is believed by the authors that the RE-containing particles near the surface are important for the oxidation process, and the detailed behavior of the particles will be shown in Sections III–D–2 and III–D–3.

2. *RE inclusion particles on sample surface of alloy F2 after oxidation*

As compared with the RE-containing particles before oxidation, after 15, 30, and 60 minutes of oxidation, the RE inclusion particles on the sample surface seemed to be covered by some oxide grains (Figure 7). The area surrounding the RE particle (between the two dotted lines in Figure 7(b) showed distinct topographical features that the oxide grains within this area were smaller than those outside of the area. On the sample oxidized

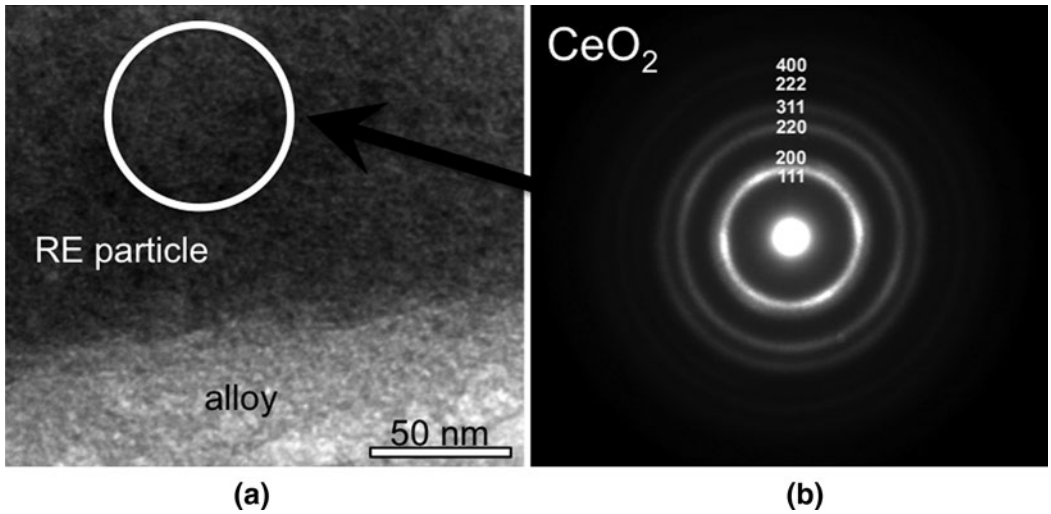

Fig. 6—(*a*) CTEM bright-field image of a RE particle and the adjacent alloy. The circle indicates the location of the selected area aperture where the diffraction patter was obtained. (*b*) Indexed selected-area diffraction pattern.

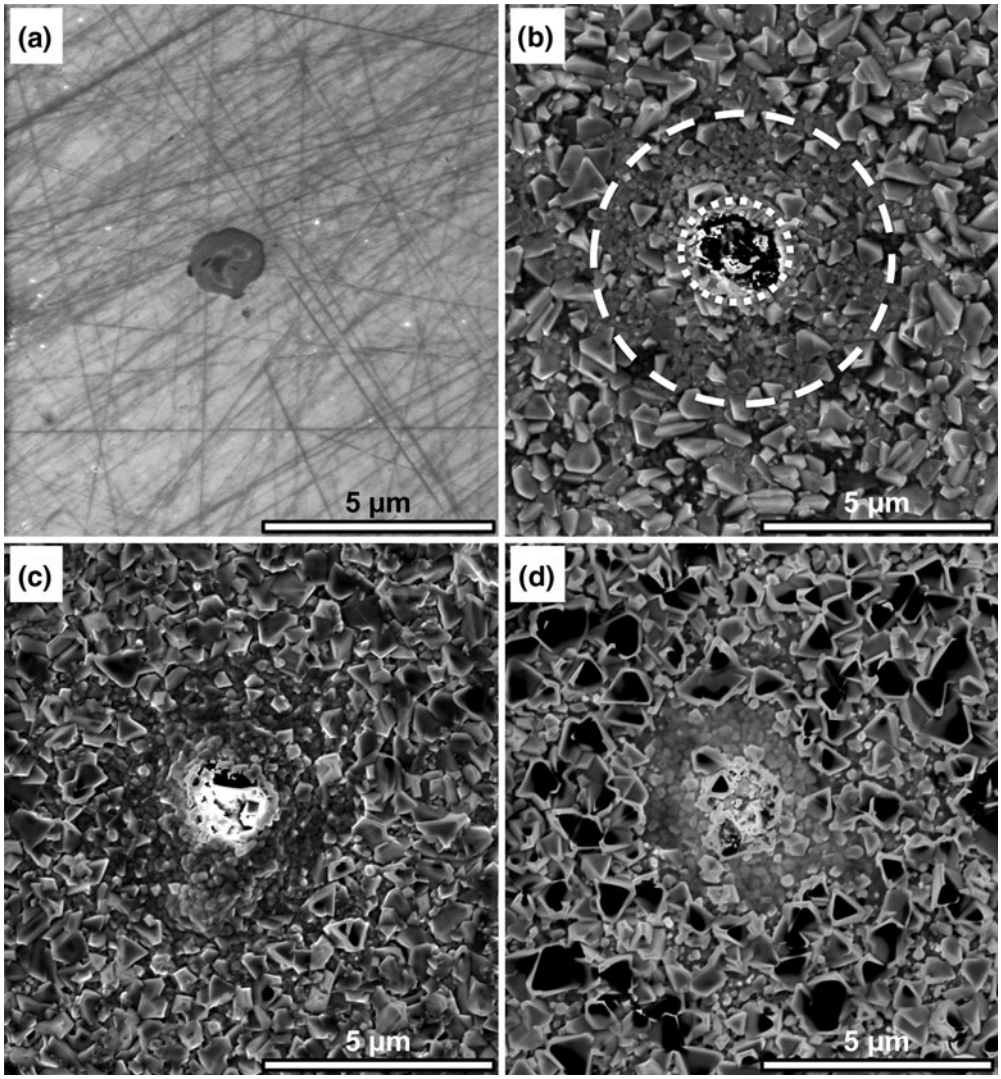

Fig. 7—Plane view SEM secondary electron images of RE-containing particles on the surface of alloy F2 (*a*) before oxidation as well as after being oxidized for (*b*) 15 min, (*c*) 30 min, and (*d*) 60 min at 1073 K (800 °C) in dry air.

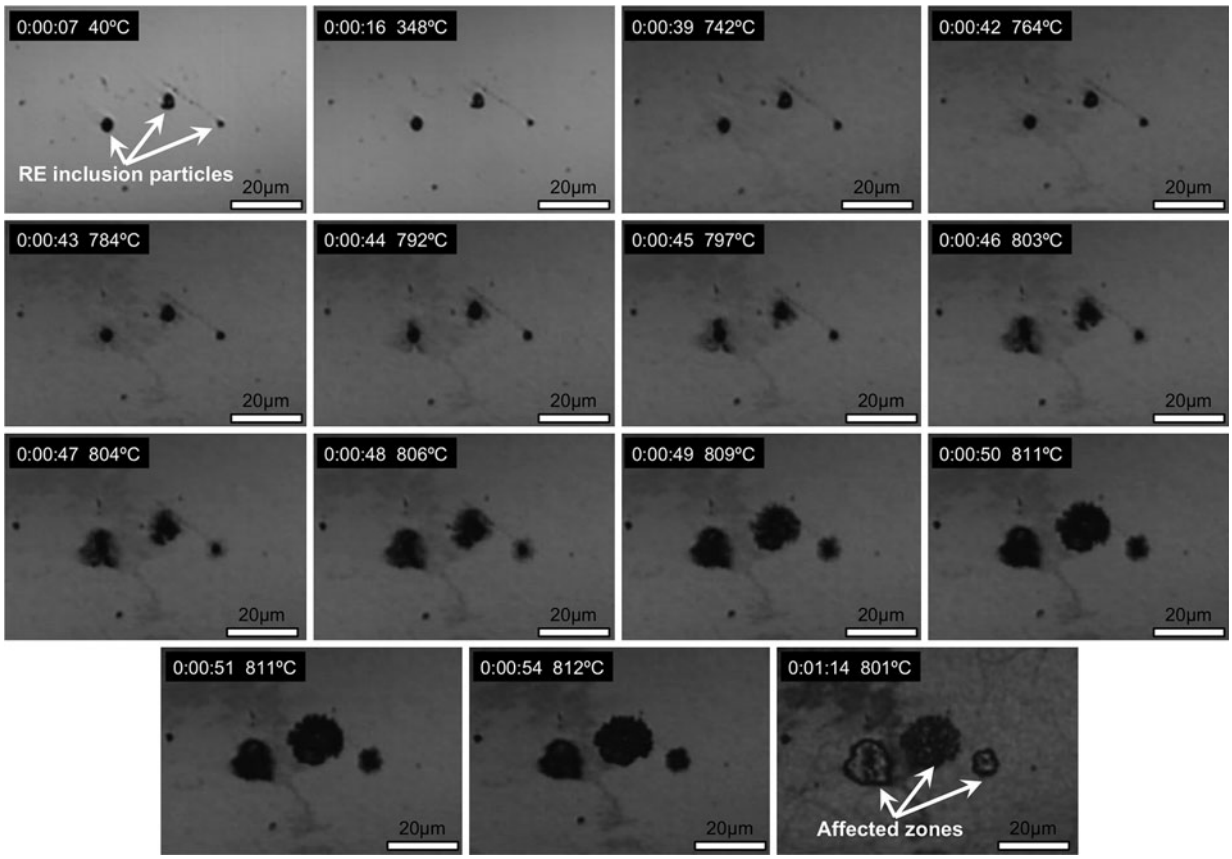

Fig. 8—CSLM still images of the formation of affected zone, extracted from real-time recorded video during the oxidation of an F3 alloy at 1073 K (800 °C) in dry air.

for 15 minutes, the Cr content in this area was determined to be approximately 30 wt pct, given by EDX, which was smaller than that of the average surface (approximately 40 wt pct). This phenomenon was named the affected zone, and it was observed on samples oxidized for up to 10 hours. Moreover, although not all RE particles on the surface had affected zones, affected zones were present in approximately 80 pct of the RE inclusions and only were present around the RE inclusions. (Because Ti sometimes also is considered a reactive element, it is possible to find an affected zone around a Ti particle.) No affected zones were found around other inclusions, such as those containing Al but no RE. The size of the affected zones varies with the size of the RE inclusion. No indication was found of whether the size of the affected zone changed with exposure time during oxidation for times up to 10 hours.

As mentioned earlier, approximately 20 pct of RE inclusions did not have affected zones, which is probably because of the different chemical composition and phases contained in each inclusion particle. For example, CeO_2 has negligible O^{2-} conductivity, but when it is doped with lanthanum, the O^{2-} conductivity can become relatively high, and the conductivity varies with the dopant content (*i.e.*, the oxygen ion transference number in ceria increases with La_2O_3 dopant content[2]). Because the RE inclusions on the sample surface are normally different from one another in terms of phases and contents, it might be the phases contained within each particle that determine the oxygen conductivity and hence determine whether an affected zone can form. However, the EDX results obtained on these particles could not show exactly which phases were contained in the particles and therefore were not conclusive evidence to support the speculation.

From the real-time observations during the oxidation experiments, it was revealed that the affected zones formed in a matter of seconds. Figure 8 shows the CSLM still images extracted from a real-time recorded video during the oxidation of an F3 alloy at 1073 K (800 °C) in dry air, with the experiment time and temperature displayed. In Figure 8, "0:00:00" corresponds to the starting point of heating; therefore, the isothermal holding starts after approximately 45 seconds, corresponding to "0:00:45."

The contrast of the CSLM images was produced as the result of the reflectivity difference between the alloy surface and the oxides, and this contrast was enhanced by surface topography.[22]

As shown in Figure 8, the oxides started to form when the temperature approached 1073 K (800 °C) (at 39 to 45 seconds). These initial oxides continued to grow quickly laterally, which is shown more clearly in the subsequent images from the time points at 45 through 49 seconds. In a simultaneous process, oxides started to grow and cover the entire alloy surface, which resulted in the darkening of the alloy surface. However, the contrast in the last few images showed that the thickness

of the scale in the affected zone must be different from the rest of the alloy surface, which was consistent with later SEM observations.

An increase of chromium and oxygen fraction within the RE-containing particles became apparent by comparing the composition of the particles before and after oxidation. This increase is likely a consequence of chromium oxides growing onto the RE particles during oxidation. Whittle and Stringer[11] reported that RE oxides dispersed on the alloy surface acted as nuclei for chromium oxides. In our experiment, RE inclusion particles are large, but they nevertheless seem to have surfaces on which chromium oxides preferentially form during the early stage of the oxidation process, which was not observed on other non-RE inclusion surfaces. This finding is consistent with the affected zone observation. Figure 9 shows the oxide grains in an affected zone, whose size ranges from approximately 50 nm to 200 nm.

Cross sections of RE inclusion particles before and after oxidation are shown in Figure 10. It is shown in Figures 10(b) and (c) that a layer has grown (white arrows) between the RE particle and the alloy during oxidation (compared with the RE particle before oxidation, Figure 10(a), wrapping up the RE particle). This layer has been identified as Cr_2O_3 by electron diffraction.*

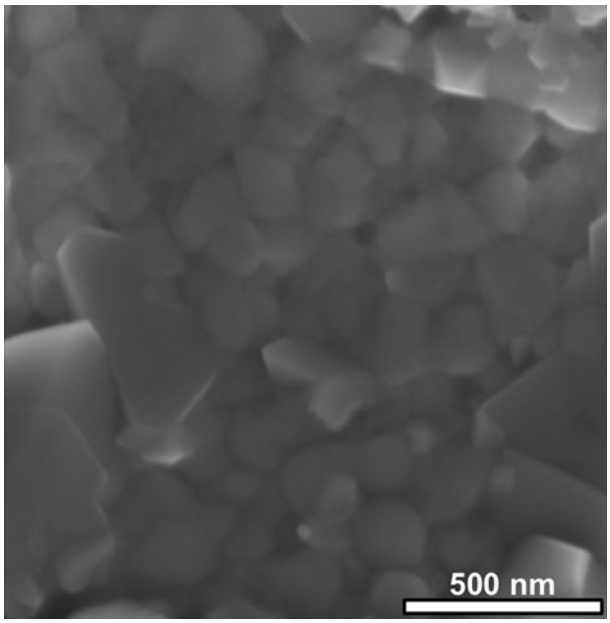

Fig. 9—A planeview SEM image of the fine-grained oxides in the affected zone on an F2 alloy oxidized for 15 min.

*To distinguish this Cr_2O_3 oxide layer wrapping the RE particle from the surface scale, it will be referred as "the layer" instead of scale.

Moreover, this layer grew thicker with an increasing oxidation time as indicated by the arrows in Figures 10(b), and (c). The cross section of the RE particles after oxidation also revealed that the thickness of the scale outside the affected zone is thicker than that of the scale inside the zone by a factor of about two.

Figure 8 shows that the size of the affected zones did not change much after approximately 50 seconds into the isothermal oxidation. The possible cause for this finding is presented in Section IV–A. When combining the cross sections of the RE-containing particles after oxidation (Figure 10), it can be speculated that 50 seconds may be the time needed to form continuous oxide layers around the RE particles.

A TEM bright-field image of a FIB lift-out cross-section specimen is shown in Figure 11. After exposure for 15 minutes to dry air at 1073 K (800 °C), a layer formed between the alloy and the RE-containing particle. The sizes of the crystals making up the layer ranged from less than 10 nm to 200 nm. A high concentration of Cr and O was determined by EDX analysis on the crystals. Electron diffraction showed that these crystals consisted of Cr_2O_3, which was consistent with the EDX spectrum. One example of the crystal and its $[48\bar{1}]$ zone axis diffraction pattern is shown in Figure 12.

Figure 13 shows a RE-containing inclusion approximately 7-μm deep into the alloy after 60 minutes oxidation at 1073 K (800 °C) in dry air, which had no contact with the free surface. Because no layer (like the layer shown in Figure 11) could be found around this particle and because the surrounding alloy composition obtained by EDX was that of the nominal composition with no RE elements found, it can be stated that RE-containing inclusion particles of this type do not participate in the oxidation or the scale-forming process until the scale has grown thick enough that the scale/alloy interface reaches

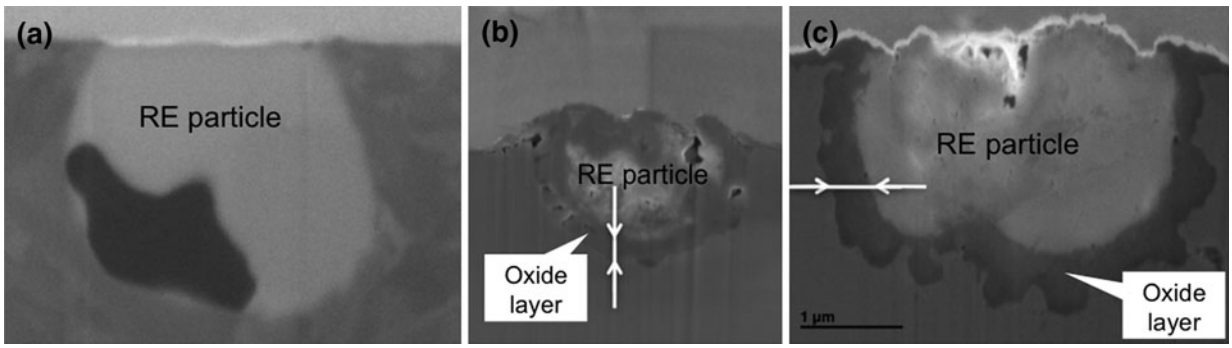

Fig. 10—Cross-sectional view of SEM secondary electron images of RE-containing inclusion particles on the surface of alloy F2 (*a*) prior to high-temperature exposure, after (*b*) 15-min and (*c*) 30-min exposure at 1073 K (800 °C) in dry air.

them. Thus, the product layer formed around the particles in Figures 11 and 12 is a result of a reaction among the gas atmosphere, the particle, and the surrounding alloy.

3. *The evolution of the location and the form of RE elements*

We assume the RE-containing particles are the starting point for oxidation changes. To track the changes in the location of RE elements, the presence of RE elements in particles was investigated as a function of distance away from the source RE particle and their location with respect to the scale/alloy interface and to the surface of the scale at two places on F2 samples oxidized for 15, 30, and 60 minutes (1) in the Cr_2O_3 layer around the RE particle and (2) in the external scale.

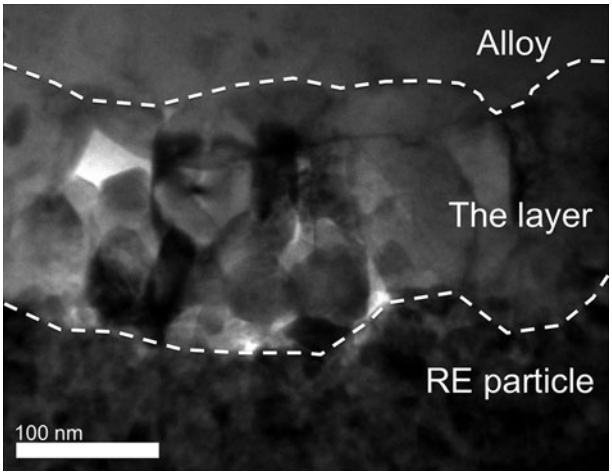

Fig. 11—CTEM bright-field cross-section image of the layer formed between the RE particle and the alloy on F2 after 15 min of exposure in dry air at 1073 K (800 °C).

a. RE elements in the "layer". The spot EDX spectra collected from the Cr_2O_3 layer around the RE particle after 15, 30, and 60 minutes of oxidation exposure disclosed the existence of the RE elements in this layer but in two distinct forms. Figure 14 is an example of the two forms of RE found. A cluster of small particles was spotted in the Cr_2O_3 layer, and they appeared with a gray level different from that of the Cr_2O_3, as circled in Figure 14(a). Quantification of EDX spectra collected from these particles show high concentrations of either Ce and/or La within each of the individual particles. It has been mentioned many times in the literature that both Ce and La are capable of forming second phases (Perovskite) with Cr_2O_3.[21,23,24] It is therefore probable that the clusters of small particles are $CeCrO_3$ and/or $LaCrO_3$. In Figure 14(b), a grain boundary between two grains in the Cr_2O_3 layer is circled. EDX compositional data obtained from the circled area showed 1.24 wt pct of Ce. Neither diffraction contrast nor phase boundaries can be seen at this location, which is an indication of the segregation of Ce ions to an oxide grain boundary and is in accordance with findings in the work by H. Fujikawa *et al.*[25]

b. RE Elements in the external scale. Figure 15 shows an example of EDX spot spectra collection in the external scale as a function of the distance away from a RE-containing particle. The numbered white circles in Figure 15 show the locations where the spectra were taken. Image drift correction was applied during each series of spectra collection to ensure accurate placement of the incident beam for EDX analyses.

As previously mentioned, the purpose of the EDX spectra collection (Figure 15) was to examine whether RE elements could diffuse into the external scale, under the assumption that the RE-containing particle acted as a "source" of RE elements.

The term "RE diffusion distance" is defined in the present study as the distance of the EDX spot analysis in the external scale farthest away from the RE-containing

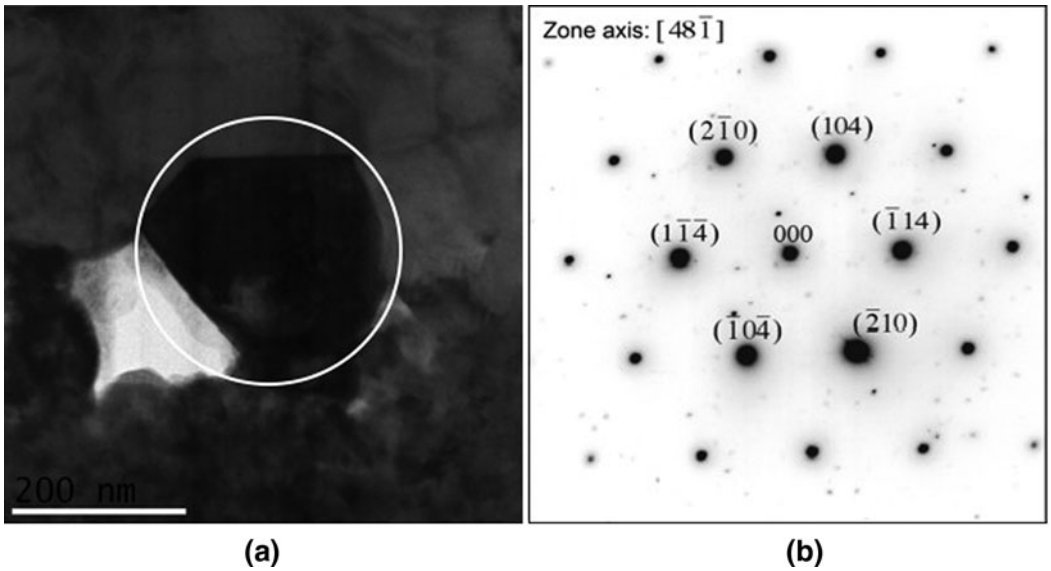

Fig. 12—(*a*) The BF image of a large grain (in the white circle) located between the RE particle and the ferritic matrix of alloy F2 oxidized for 15 min at 1073 K (800 °C), in dry air. (*b*) Indexed zone axis diffraction pattern of this circled grain.

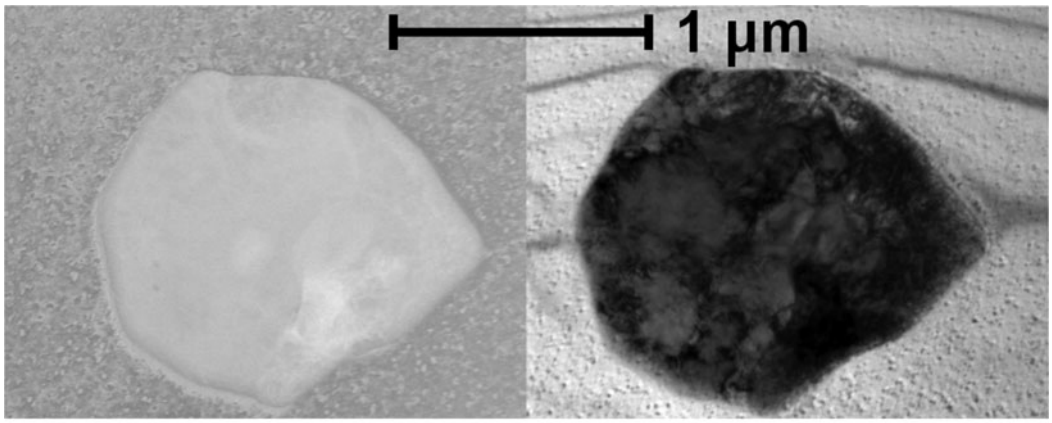

Fig. 13—(*a*) STEM HAADF image and (*b*) CTEM bright-field image of a RE-containing inclusion inside the F2 alloy with no contact to the free surface (approximately 7 μm to the free surface) after 60 min high-temperature exposure at 1073 K (800 °C) in dry air.

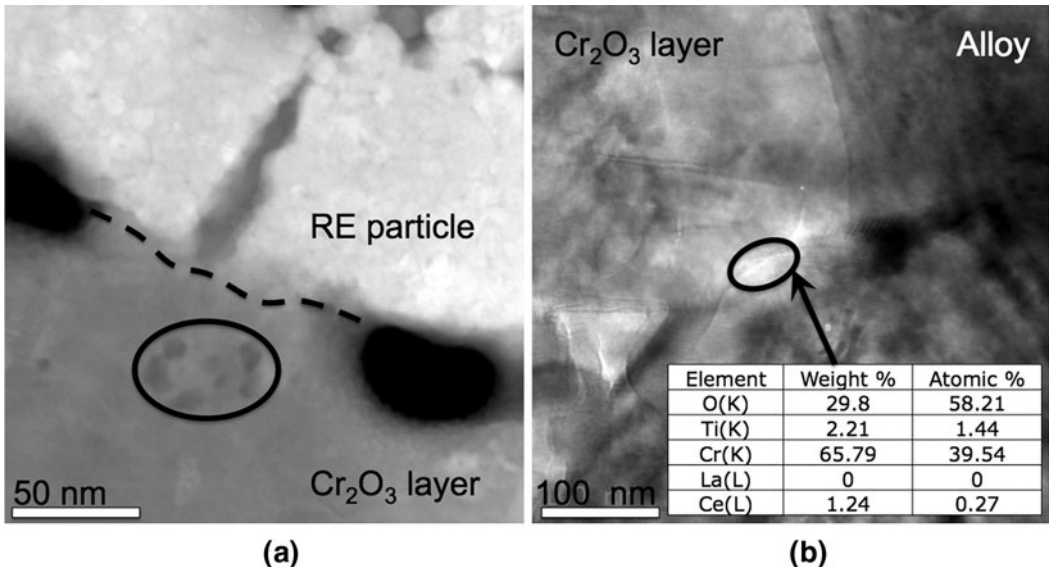

Fig. 14—(*a*) STEM HAADF cross-sectional image of the Cr_2O_3 layer between the RE particle and the alloy (F2, oxidized for 30 min at 1073 K [800 °C] in dry air). The circled is a cluster of small particles in the Cr_2O_3 layer. (*b*) CTEM bright-field image of the Cr_2O_3 layer between the RE particle and the alloy (F2, oxidized for 15 min at 1073 K [800 °C] in dry air). The circled is a grain boundary between two Cr_2O_3 grains in the layer. EDX spectrum collected from the circled area showed 1.24 wt pct of Ce.

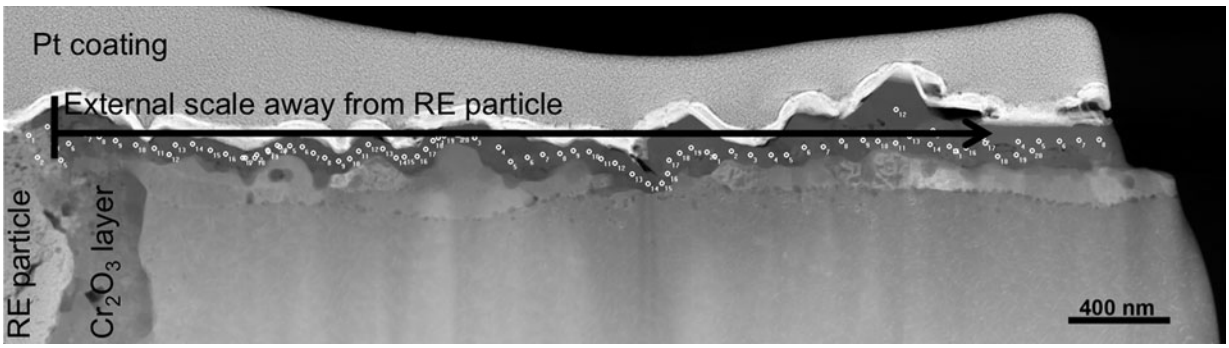

Fig. 15—STEM HAADF cross-sectional image of the external scale on alloy F2 (Fe-22Cr-0.04RE) oxidized for 30 min at 1073 K (800 °C) in dry air. The white circles indicate the locations where EDX spot analyses were performed.

particle where a significant RE signal is obtained. The spots farther than this point have zero RE signal through the edge of the specimen. The RE diffusion distance measured on the RE-containing inclusion particle oxidized for 15, 30, and 60 minutes are summarized in Figure 16; for the sample that underwent 15 minutes exposure, this distance is about 400 nm on either side of the RE particle in the external scale; for the samples oxidized for 30 and 60 minutes, the distance for each is approximately 800–1000 nm.

To clarify the location of RE in the scale layer, vertical line scans across the scale/alloy interface and the scale/gas interface and the oxide grain boundaries by STEM-EDX were performed on specimens oxidized for 30 and 60 minutes.

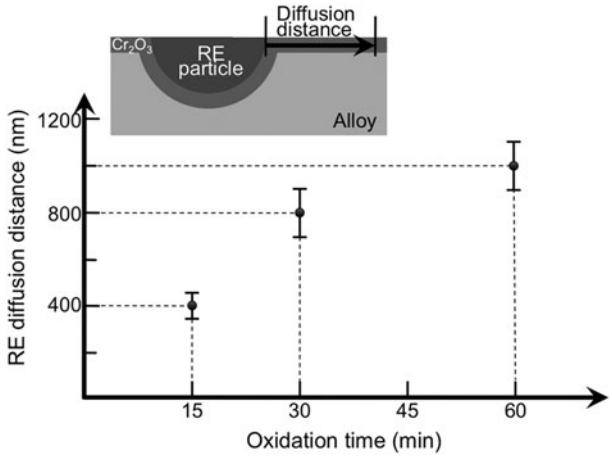

Fig. 16—The diffusion distance of RE elements in the external scale with increasing oxidation time in F2 alloy based on the observations with TEM and EDX.

Figures 17 and 18 are two examples of two different measurements; one is a line scan across alloy/scale and scale/gas interfaces, and the other is a line scan across two oxide grains.

In Figure 17(a), a STEM image is shown along with a line labeled AB, the location where the line scan was performed, and the integrated intensities of La, Ce, and Pt are plotted with the location of the interfaces indicated by the two dotted lines (Figure 17(b)). On the specimen oxidized for 30 minutes, a higher intensity of Ce and/or La was found on the interfaces (*i.e.*, scale/alloy interface and the scale surface). In a few cases, Ce was found between the two interfaces, within the scale. The vertical line scans performed on the specimen oxidized for 60 minutes gave similar results as those of a specimen oxidized for 30 minutes. It is also interesting to note that, in all vertical line scans acquired so far on both specimens, La has been found on both interfaces but seldom has been found in the scale. Ce, however, was found occasionally within the scale.

As Ce has been found in the scale, it is of interest to determine whether Ce existed inside the oxide grains or at the oxide grain boundaries; therefore, line scans across two adjacent grains also were performed on samples oxidized for 30 and 60 minutes, which showed the presence of RE elements at grain boundaries for both oxidation times. One example line scan across two adjacent oxide grains is shown in Figure 18, whose quantification shows a peak intensity of Ce at the grain-boundary location. No La signal was found in this particular case. RE elements found at oxide grain boundaries are consistent with many published works, and such segregation of the RE elements at the scale oxide grain boundaries widely was believed to be the source of suppression of cation diffusion as well as of the promotion of the contribution of anion diffusion to the scaling process.[14,25]

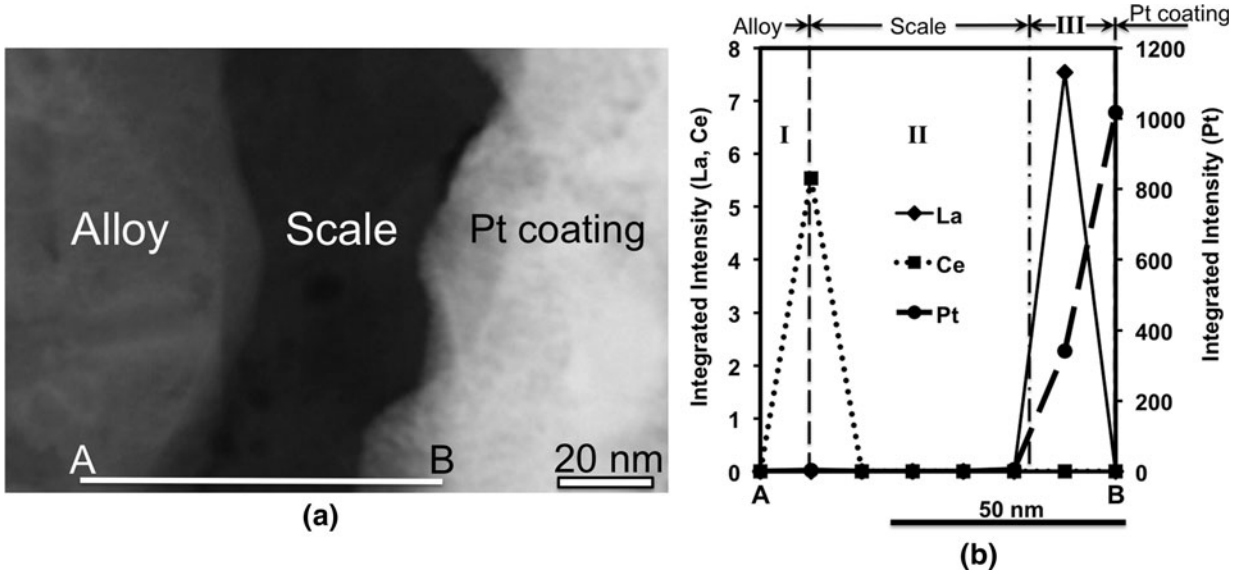

Fig. 17—(*a*) STEM HAADF cross-sectional view image of the alloy F2 (Fe-22Cr-0.04RE) oxidized for 60 min at 1073 K (800 °C) in dry air. The line AB indicates the position where the line scan was performed. (*b*) Integrated intensity of the line scan along the line AB shown in (a). Region I is the alloy; region II is the external scale; region III is the interface between scale and Pt coating, which is actually the scale surface in a high-temperature exposure.

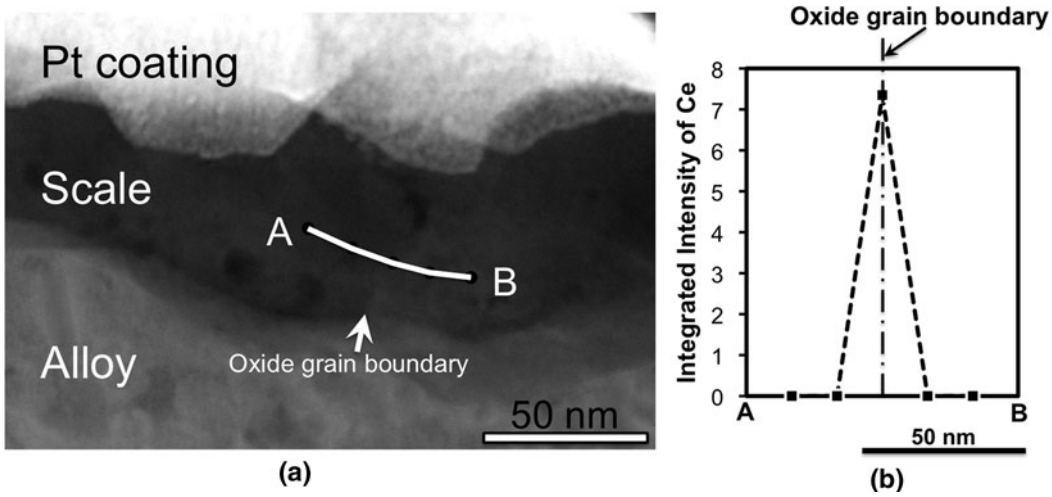

Fig. 18—(*a*) STEM HAADF cross-section view image of the alloy F2 (Fe-22Cr-0.04RE) oxidized for 60 min at 1073 K (800 °C) in dry air. The line AB indicates the position where the line scan was performed. (*b*) Integrated intensity of the STEM-EDX line scan along the line AB shown in (a).

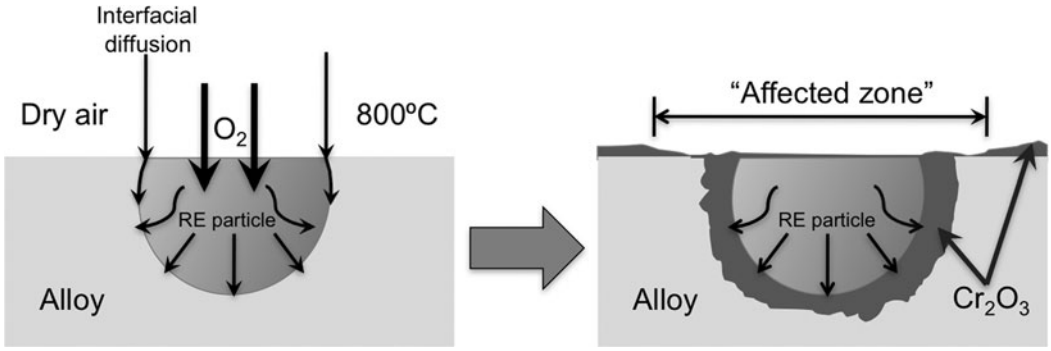

Fig. 19—Schematic of the formation of the affected zone.

IV. DISCUSSION

Because the location of RE in the oxide scale is essential to understanding the role of RE in the REE, the results shown in Section III will be discussed in light of the mechanisms proposed in the literature, such as grain-boundary segregation theory and the poisoned interface mechanism (PIM).

A. *Affected Zone*

The affected zone (Figures 7 and 8) has not been investigated or discussed in detail in the literature. However, the fact that the initial specific mass gain of the F2 alloy was slightly greater than that of the base alloy[15] suggested that the formation of affected zones around RE particles might be the cause.

The affected zones formed rapidly during the early stages of oxidation (the first few minutes) as noted through real-time observation with CSLM (Figure 8). Although it was shown that the surface scale in the affected zone was considerably thinner than the scale outside the zone, a layer of Cr_2O_3 formed around the RE particle, which only could be observed in the cross section. This Cr_2O_3 layer usually had a thickness comparable with or even larger than that of the scale outside the affected zone.

It is believed that the high oxygen-ion conductivity of some RE compounds, such as La_2O_3 doped CeO_2 that was used as the electrolyte of a SOFC for transporting oxygen ions,[2] may have played a key role in the formation of the Cr_2O_3 layer around the RE particle and hence the affected zone on the scale surface. Figure 19 shows a schematic drawing of a possible course of formation for an affected zone. When high-temperature exposure begins, and because oxygen can diffuse easily through the RE inclusion, Cr within the ferritic matrix surrounding the RE particle is oxidized rapidly. Consequently, this region is depleted rapidly of scale-forming elements (mostly Cr), leading to an affected zone on the surface. With the depletion of Cr in the ambient alloy near the particle, no Cr can suffice the scale in the affected zone to grow thicker, which is likely the reason why the affected zone stops growing larger in Figure 8 after approximately 50 seconds into the isothermal oxidation. It also should be noted that the interface between the inclusion particle and the alloy may result in an inward interfacial diffusion of oxygen

that also can oxidize the Cr around the particle. However, the affected zone so far was observed only around RE-containing particles, and hence, either the RE-containing particles form an interface with the matrix that is a fast path for oxygen transport compared with other particles or the these interfaces are not contributing appreciably to the transport when compared with the transport through the RE-particles themselves.

Moreover, Stringer and Wright[26] reported that, when fine particles of RE oxides were dispersed onto the alloy surface, they became preferential nucleation sites for alloy oxides in the first stage of oxidation and resulted in a fine-grained scale (nucleation effect).In the current study in which metallic RE was added into the bulk alloy, fine scale grains only were found in the area surrounding the RE-containing particles instead of the entire surface. This finding suggests that some unique surface properties of the RE particles must cause the nucleation effect both reported by Stringer and Wright and observed in this study.

Although the depletion of Cr in a localized area may lead to the formation of nonprotective surface Fe oxides (which has not been observed for exposure times up to 60 minutes), fast formation of an oxide layer around RE particles can shorten the time required for nuclei to grow into a continuous chromia oxide layer by which the bulk alloy is protected in steady-stage oxidation. Therefore, the curtailing of the transient stage[11] as well as the faster transition from transient to the steady state of oxidation observed on alloys with metallic RE addition may be a result of the formation of the affected zone.

B. *Evolution of Microstructural Features (Second-Phase Particles, or Segregation) that Contain RE*

1. *Diffusion of RE into the scale*

TEM-EDX observations (Figures 16 through 18) on RE particles in the F2 alloy as a function of oxidation time revealed that RE in the RE particles did not remain stationary during oxidation; instead, they diffused into the C_2O_3 layer and the external scale. Thus, the particles serve as sources of RE that migrate into the Cr oxide scale. It is postulated that the driving force for this diffusion is the RE concentration difference between the particle and the scale.

Although no diffusion data of La and Ce in Cr_2O_3 are available in the literature and because it is difficult to measure a continuous concentration profile of RE in the scale, an approximate diffusion coefficient of RE, D_{RE}, can be calculated from the "diffusion distance" described in Figure 16 by assuming a semi-infinite system as distance is extended along the scale, starting from the particle/scale interface. The obtained value of the "diffusion coefficient" then can be compared with available diffusion coefficients of yttrium in Cr_2O_3 that has been reported in the literature.[27] This comparison would suggest whether the proposed diffusion mechanism of RE in the external scale is reasonable to a first approximation.

In this semi-infinite model, the size of the RE particle is large enough to serve as a constant source and the external

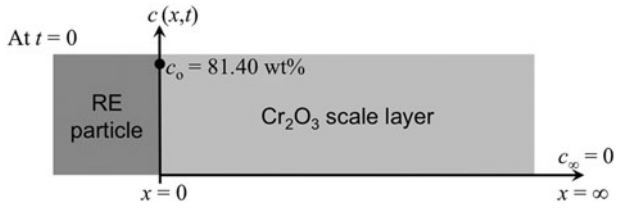

Fig. 20—Schematic drawing of the semi-infinite model incorporated into experimental setup.

scale layer can be assumed to be initially diffusant-free. The concentration of RE as a function of distance and time, $c(x,t)$, is given by the following Eq. [1][28]:

$$c(x,t) = c_0 \mathrm{erfc}\left(\frac{x}{2\sqrt{Dt}}\right) \quad [1]$$

where x is the distance away from the source of the diffusant, t is time, c_0 is the concentration at $x = 0$, and D is the diffusion coefficient. Values for time and the $c(x, t)$ were determined experimentally from EDX analysis and are $t = 60$ minutes and $c(x,t) = c(800\ \text{nm}, 60\ \text{minutes}) = 1$ pct. According to the assumptions in the semi-infinite model, the boundary condition is set as $c_0 = 81.40$ wt pct at $x = 0$, which is the weight percent of Ce in CeO_2. The conditions at $t = 0$ are depicted in Figure 20. Solving Eq. [1] for the diffusion coefficient results in a value of $D_{RE} = 1.42 \times 10^{-17}$ m^2/s for RE in Cr_2O_3 at 1073 K (800 °C).

J. Li *et al.*[27] measured the bulk and grain boundary diffusion coefficients of Y in Cr_2O_3, and the values are $D_{0,GB} = 2.56 \times 10^{-8}$ (m^2/s) and $Q_{GB} = 190$ (kJ/mol); $D_{0,lattice} = 1.20 \times 10^{-15}$ (m^2/s) and $Q_{lattice} = 144$ (kJ/mol). Q is the diffusion activation energy. At 1073 K (800 °C), the following is true:

$$D = D_0 e^{-\frac{Q}{RT}} \quad [2]$$

$$D_{GB,yttrium} = 1.44 \times 10^{-17}\ \mathrm{m}^2/\mathrm{s}$$

and

$$D_{lattice,yttrium} = 1.17 \times 10^{-22}\ \mathrm{m}^2/\mathrm{s}.$$

Comparing the approximated D_{RE} ($D = 1.42 \times 10^{-17}$ m^2/s) with the diffusion coefficients of yttrium in chromia grain boundaries, it is shown that $D_{RE} \approx D_{GB,yttrium}$. It is evident from this calculation that the diffusion of RE from the particle cannot take place by bulk diffusion through the scale because D_{RE} is five orders of magnitude greater than $D_{bulk,yttrium}$. Also, the TEM-EDX analysis in the bulk oxides in the external scale did not show any evident RE signal. It is therefore likely that RE diffuses into the scale predominantly through grain boundary diffusion. Moreover, the fine Cr_2O_3 grains in the affected zone correlate well with such grain-boundary diffusion.

According to T. Akashi *et al.*,[29] La and Ce should diffuse slower than Y in the same oxide because of their larger ionic radius as well as a higher charge carried by Ce^{4+}. However, the calculated D_{RE} is about the same as the value of $D_{GB,yttrium}$ given by Reference 27.

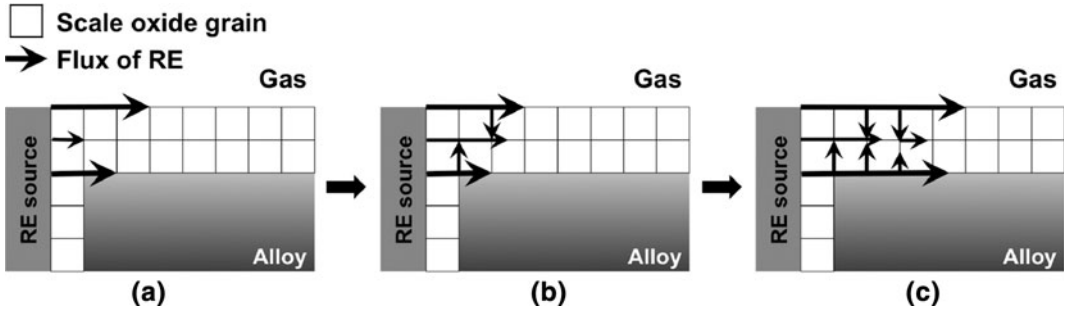

Fig. 21—Schematic drawing of the diffusion of RE from the source into the scale during a high temperature exposure. (*a*) RE ions begin to diffuse into external scale along metal/scale interface, oxide grain boundaries and scale surface. (*b*) Some RE ions may enter oxide grain boundaries from metal/scale interface and/or scale surface. (*c*) Continuation of both interfacial diffusion and grain-boundary diffusion of RE ions as the oxidation proceeds.

According to TEM-EDX results (Figure 17), La and Ce also were found along the metal/scale and scale/gas interfaces. Because the metal/scale interface may be more disordered than the oxide grain-boundary interfaces, it can be expected that the RE diffusion along the metal/scale interface should be easier than the scale/gas interface. It also could be possible that the RE is transported along the scale surface. Therefore, fast interfacial diffusion may result in a calculated D_{RE} about the same magnitude as $D_{GB,yttrium}$.

Based on the previous analysis, the authors proposes a mechanism to explain the diffusion of RE in the scale, which is displayed schematically in Figure 21. A few minutes after the isothermal oxidation starts, a thin scale forms on the alloy surface as well as around the RE particle (the affected zone). Once contact is made between the RE inclusion and the oxides, the RE ions begin to diffuse out of the RE particle source, possibly by both interfacial and grain-boundary diffusion (Figure 21(a)), under a driving force of the concentration difference inside and outside the particle. As shown in Figure 6, the self-diffusion of RE elements in the nanocrystalline RE particle must be fast because of a large grain-boundary interface area, which means that the supply of RE elements to the particle/scale interface is never exhausted, at least in the oxidation times considered in this study. Some RE ions also may enter oxide grain boundaries that intersect the metal/scale and/or scale/gas interface, (Figure 21(b)). As the high-temperature exposure proceeds, the RE ions enter more oxide grain boundaries while the two interfacial RE fluxes go farther into the external scale (Figure 21(c)).

2. *Relation between observed diffusion of RE into the scale and reduced scale growth rate*

As the oxidation of the alloy proceeds for longer times, the RE content in inclusion particles, which are acting as sources, would be decreasing and consequently the flux of the RE ions would decrease. Because the inclusions are spaced far apart and not in a homogeneous manner, it may seem unlikely that enough RE would be present to influence the properties of the entire bulk of the scale as time progresses. The following possible explanations could be considered to explain this finding:

(a) It is possible that the RE ions segregate to either the interfaces or grain boundaries within the scale and are thereby able to influence a greater volume of the scale. Because of the large ionic radius difference between RE elements and alloy host elements, it commonly is accepted that the solubility of RE ions in a chromia scale is negligibly low.[30] Therefore, if the RE ions are present in the chromia scale, they must be present at the oxide grain boundaries. Such an occurrence would support the following popular mechanisms proposed in the literature: (1) the RE ions that segregate to the oxide grain boundaries block grain-boundary diffusion,[13,31] and (2) the RE segregation to the oxide/metal interface slows the interface reaction.[32] Although the exact mechanism through which RE ions prohibit diffusion along oxide grain boundaries is not presently agreed on, it is well acknowledged that such segregation suppresses grain boundary diffusion resulting in significant reduction of the scale growth rate below 1273 K (1000 °C) when grain-boundary diffusion accounts for approximately 90 to 100 pct of transport through the scale.[20] The presence of the RE ions may reduce the amount of scale forming Cr-ions at the boundaries and consequently may reduce their outward flux and scale growth.

(b) It is possible that interactions take place between RE ions and defects at grain boundaries, which create complex defects that reduce the mobility of point defects critical for transport through the scale. If the difference in size and electron affinity of RE ions produce defect pairs or even clusters in the boundary,[33] limiting the mobility of migrating species, or if the introduction of misfitting ions into a grain boundary change the defect's migration path as a result of the physical distortion, then the activation energy of migration along the grain boundary consequently may increase.[33] Through defect model calculation, Duffy and Tasker[34] showed that the presence of an isolated Ce^{4+} ion in an oxide grain boundary increases the activation energy for the diffusion of vacancies to a value greater than the activation energy of bulk diffusion. In perspective, a precise comprehension

of the defect nature in the chromia scale can improve greatly the understanding of incorporation of RE ions at the oxide grain boundaries.

(c) The presence of RE elements at the scale/metal interface may have an impact on the injection of scale-forming ions into the scale if the PIM is correct. Proposed by B. Pieraggi *et al.*,[32] the PIM stated that the interfacial segregation of large reactive element ions could inhibit the climbing and/or gliding of interface dislocations and thus could block a crucial step in the scale-forming reaction—creation and/or annihilation of point defects (*i.e.*, vacancies and interstials). If the misfit dislocations and the misorientation dislocations of the metal cannot climb and thereby annihilate vacancies (or create metal interstitial ions for other scale-metal systems), then the classic Wagner model with the interfacial reactions at local equilibrium is not valid. Likewise, an equilibrium within the scale for cations and anions, and their defect species, cannot be satisfied. Furthermore, if large segregated RE ions block the annihilation of cation vacancies required to support cation transport in the scale, then the anionic scale growth would replace normal cationic scale growth, as is observed for the REE for chromia growth. However, because of the oxygen partial pressure imposed on the thickness direction of the scale as well as the simultaneous migration of cations and anions, the defect structure at the scale/metal interface may be complicated.

At this stage, we do not have sufficient information to identify the exact mechanism for restricting scale growth induced by the RE elements. A more detailed study into the defect structure of the grain boundaries and the scale/metal interface would be required to show which mechanisms are responsible for the decreased scale growth rate.

V. SUMMARY

The behavior of an Fe-22Cr-0.04RE alloy during transient oxidation at 1073 K (800 °C) in dry air was studied, and the evolution of the scale and RE-containing features was elucidated. The formation of affected zones around the RE particles was investigated, and their possible relation to oxidation kinetics was discussed. RE diffused into the scale from the RE particles on the alloy surface during the high-temperature exposure. Based on the location of RE in the scale, it is proposed that the RE diffused into the scale by both diffusion along the metal/scale and scale/gas interfaces as well as the oxide grain boundaries, which seemed to be supporting evidence for both the oxide grain-boundary segregation theory and the PIM.

ACKNOWLEDGMENTS

This technical effort was performed in support of the NETL's ongoing research in the study of the effects of rear earth elements on the high-temperature oxidation of stainless steels under the RES contract DE-FE0004000. The authors would like to acknowledge the excellent technical support on electron microscopy of Tom Nuhfer.

REFERENCES

1. W.J. Quadakkers, J. Piron-Abellan, V. Shemet, and L. Singheiser: *Mater. High Temp.*, 2003, vol. 20 (2), pp. 115–27.
2. N.Q. Minh and T. Takahashi: *Science and Technology of Ceramic Fuel Cells*, Elsevier, New York, NY, 1995, pp. 12–13, 92–93.
3. P. Y. Hou, K. Huang, and W. T. Bakker: in *Solid Oxide Fuel Cells (SOFC VI)*, S.C. Singhal and M. Dokiya, eds., The Electrochemical Society Proceedings Series, Pennington, NJ, 1999, p. 737.
4. Crofer 22 APU Material Data Sheet No. 4046, June 2008 Edition, ThyssenKrupp VDM, Southfield, MI, 2008.
5. P. Huczkowski, N. Christiansen, V. Shemet, J. Piron-Abellan, L. Singheiser, and W.J. Quadakkers: *J. Fuel Cell Sci. Technol.*, 2004, vol. 1, pp. 30–34.
6. R. Hojda, W. Heimann, and W.J. Quadakkers: *ThyssenKrupp Techforum*, 2003, pp. 20–23.
7. J.J. Choi, J.H. Ryu, B.D. Hahn, W.H. Yoon, B.K. Lee, J.H. Choi, and D.S. Park: *J. Alloys Compd.*, 2010, vol. 492 (1–2), pp. 488–95.
8. E.A. Lee, J.S. Yoon, H.J. Hwang, J.W. Moon, and N.U. Cho: *J. Ceram. Process. Res.*, 2008, vol. 9 (5), pp. 538–43.
9. P. Kofstad: *High-Temperature Oxidation of Metals*, Wiley, New York, NY, 1966, pp. 11–19.
10. N. Bricks, G.H. Meier, and F.S. Pettit: *Introduction to the High-Temperature Oxidation of Metals*, 2nd ed., Cambridge University Press, Cambridge, UK, 2006, pp. 39–40.
11. D.P. Whittle and J. Stringer: *Philos. Trans. R. Soc. London, Ser. A*, 1980, vol. 295 (1413), pp. 309–29.
12. L.B. Pfeil: UK Patent, No. 459 848, 1937.
13. G.M. Ecer and G.H. Meier: *Oxid. Met.*, 1979, vol. 13, pp. 159–80.
14. Z. Tang, S. Chumbley, E. Kalay, and B. Gleeson: Oral Presentation at TMS Annual Meeting 2009, San Fransico, CA, 2009.
15. D.E. Alman and P.D. Jablonski: *Surface Modifications for Oxidation Resistance, Eighth Annual SECA Workshop*, San Antonio, TX, 2007.
16. J. Zhu, L.M. Fernandez Diaz, G.R. Holcom, P.D. Jablonski, C.J. Cowen, D.E. Laughlin, D. Alman, and S. Sridhar: *J. Electrochem. Soc.*, 2010, vol. 157 (5), pp. B655–64.
17. L.M. Fernandez Diaz, J. Zhu, G.R. Holcomb, P.D. Jablonski, D.E. Alman, and S. Sridhar: *Def. Diff. Forum*, 2009, vols. 283–286, pp. 425–31.
18. Z. Yu: *The Application of Rare Earth in Iron and Steels*, Metallurgical Industry Press, Beijing, PR China, 1987, pp. 251–61.
19. D.A. Porter and K.E. Easterling: *Phase Transformation in Metals and Alloys*, 2nd ed., Taylor & Francis Group, Boca Raton, FL, 2004, pp. 179–99.
20. E.A. Polman, T. Fransen, and P.J. Gellings: *J. Phys. Condens. Matter*, 1989, vol. 1, pp. 4497–510.
21. D.A. Downham and S.B Shendye: *Oxid. Met.*, 1995, vol. 43, pp. 411–33.
22. C. Thorning and S. Sridhar: *Philos. Mag.*, 2007, vol. 87, pp. 3479–99.
23. S.B Shendye and D.A. Downham: *Oxid. Met.*, 1995, vol. 43, pp. 435–57.
24. K. Przybylski and G.J. Yurek: *Mater. Sci. Forum*, 1989, vol. 43, pp. 1–74.
25. H. Fujikawa, T. Morimoto, Y. Nishiyama, and S.B. Newcomb: *Oxid. Met.*, 2003, vol. 59, pp. 23–40.
26. J. Stringer and I.G. Wright: *Oxid. Met.*, 1972, vol. 5, pp. 59–84.
27. J. Li, M.K. Loudjani, B. Lesage, and A.M. Huntz: *Phil. Mag. A*, 1997, vol. 76, pp. 857–69.
28. I. Kaur, Y. Mishin, and W. Gust: *Fundamentals of Grain and Interphase Boundary Diffusion*, 3rd ed., Wiley, New York, NY, 1995, pp. 6–7.
29. T. Akashi, M. Nanko, and T. Maruyama: *J. Electrochem. Soc.*, 1998, vol. 145, pp. 2090–94.
30. B.A. Pint: *John Stringer Symposium on High Temperature Corrosion: Proc. from Materials Solutions Conf. 2001*, ASM International, Indianapolis, IN, 2001, p. 9.

31. R. Haugsrud, A.E. Gunnaes, and C.R. Simon: *Oxid. Met*., 2001, vol. 56, pp. 453–65.
32. B. Pieraggi, R.A. Rapp, and J.P. Hirth: *Oxid. Met*., 1995, vol. 44, pp. 63–79.
33. R.W. Jackson, J.P. Leonard, F.S. Pettit, and G.H. Meier: *Solid State Ionics*, 2008, vol. 179, pp. 2111–20.
34. D.M. Duffy and P.W. Tasker: *Philos. Mag. A*, 1986, vol. 54, pp. 759–71.